SOFT ROBOTS

Electronics-free pneumatic circuits for controlling soft-legged robots

Dylan Drotman[1], Saurabh Jadhav[1], David Sharp[1], Christian Chan[1], Michael T. Tolley[1,2]*

Pneumatically actuated soft robots have recently shown promise for their ability to adapt to their environment. Previously, these robots have been controlled with electromechanical components, such as valves and pumps, that are typically bulky and expensive. Here, we present an approach for controlling the gaits of soft-legged robots using simple pneumatic circuits without any electronic components. This approach produces locomotive gaits using ring oscillators composed of soft valves that generate oscillating signals analogous to biological central pattern generator neural circuits, which are acted upon by pneumatic logic components in response to sensor inputs. Our robot requires only a constant source of pressurized air to power both control and actuation systems. We demonstrate this approach by designing pneumatic control circuits to generate walking gaits for a soft-legged quadruped with three degrees of freedom per leg and to switch between gaits to control the direction of locomotion. In experiments, we controlled a basic walking gait using only three pneumatic memory elements (valves). With two oscillator circuits (seven valves), we were able to improve locomotion speed by 270%. Furthermore, with a pneumatic memory element we designed to mimic a double-pole double-throw switch, we demonstrated a control circuit that allowed the robot to select between gaits for omnidirectional locomotion and to respond to sensor input. This work represents a step toward fully autonomous, electronics-free walking robots for applications including low-cost robotics for entertainment and systems for operation in environments where electronics may not be suitable.

INTRODUCTION

Recently, soft robots that use flexible materials and structural compliance to achieve complex movements have demonstrated promise for simplifying interactions with complex environments and for safely interacting with humans (*1*). Various approaches have been presented for the actuation of soft robots, including systems driven by pneumatic (*2*) or hydraulic pressure (*3*), tendons (*4*), or smart materials (*5*, *6*). Pneumatic actuation is particularly attractive for many applications due to the low fabrication complexity and the commercial availability of the required components (*7*). Generally, this approach involves inflating a sealed chamber within a soft body with a controlled supply pressure. A material or geometric asymmetry then causes the soft body to move in a prescribed direction (e.g., bending, twisting, and extension/contraction).

The ability of soft robots to adapt to variable terrain makes them attractive for locomotion. We have previously found that a pneumatically actuated soft-legged robot with three actuated DoFs per leg was able to navigate a variety of terrains (e.g., flat or valley-shaped, covered with loose rocks or pebbles) using very simple gait patterns (*8*, *9*). The compliance of the soft limbs of the robot also enabled it to squeeze into tight spaces (*8*). When augmented with an inflatable soft body, we further demonstrated that the robot was able to manipulate the hydrodynamic forces it experienced while walking underwater to improve locomotion for a variety of ambient flow conditions (*10*).

Previous pneumatically or hydraulically powered soft robots that use rhythmic motion to achieve locomotion [e.g., by walking (*2*, *8*, *9*, *11*), crawling (*12*), rolling (*13*), slithering (*14*), swimming (*3*, *15*, *16*), peristaltic digging (*17*, *18*), or jumping (*19*)] have been primarily controlled by pumps and/or solenoid valves connected to an electronic microcontroller. For example, we used a modified version of an open-source fluidic control board (*20*) to control the movement of our previous soft-legged robot (*8*). We, and others, have also used closed volume actuation systems (e.g., pneumatic or hydraulic pistons) to supply both positive and negative pressure for controlling soft robotic systems (*21*, *22*).

Despite these demonstrations, two major challenges for fluidic soft robots are the size and the cost of the components (e.g., electronics, pumps, and valves) required for their actuation and control (*7*). Because at least one pump or valve is required per actuated DoF, the size and cost of these components place a lower limit on the size of soft robots and an upper limit on the number of actuated DoFs.

To address these limitations, recent work has investigated fluidic control circuits for soft robots. In these circuits, simple fluidic components [e.g., microfluidic valves (*23*)] can replace relatively large and expensive electromagnetic components (e.g., solenoid valves). Previous work used microfluidic valves to interface with computer-controlled Braille displays consisting of 64 solenoid valves to independently actuate 32 pneumatic DoFs (*24*). Recent work has used microfluidic demultiplexers to decrease the number of solenoid valves required per independently controlled fluidic lines (to n valves for 2^n lines) (*25*). The disadvantage of demultiplexing schemes is that only one of the outputs can be controlled at a time, limiting the temporal resolution of actuation.

Garrad *et al.* (*26*) developed an alternative type of fluidic circuit that converts sequences of conductive and dielectric fluids into analog or digital signals that can be used to generate sequences of actuation to control soft robots such as a soft worm. This approach has the potential to reduce some of the components (e.g., valves) required to control a soft robot but still relies on a combination of fluidic and electrical components and has yet to demonstrate control of complex soft-legged robot.

To reduce the cost and complexity of soft machines and to enable applications in environments at risk of spark ignition (e.g., in

[1]Department of Mechanical Engineering, University of California, San Diego, La Jolla, CA 92093, USA. [2]Materials Science and Engineering Program, University of California, San Diego, La Jolla, CA 92093, USA.
*Corresponding author. Email: tolley@ucsd.edu

underground mines), recent work has investigated fluidic circuits for controlling electronics-free soft robots. This work builds on a rich area of research on the design of integrated microfluidic circuits for signal generation and computation (*27*–*32*). Integrating an oscillating microfluidic circuit into a soft body has led to a fully soft untethered robot that used monopropellant decomposition to power a simple motion pattern (*33*). However, this work did not present an approach to control complex motions (such as the gait cycles of a legged robot), and the physical dimensions of the microfluidic channels limited the fluid flow rate—and hence power—of the actuators. Recent work took a step toward a microfluidic controller for legged robots (*34*). With power, control, and clock inputs, this work demonstrated the selection of states (walking or grasping) for a rigid robot. However, this work did not address the generation of clock signals or an approach to enable sufficient fluid flow to actuate a soft robot.

Rothemund *et al.* (*35*) developed bistable valves that enabled sufficient fluid flow for controlling pneumatic soft robotic devices such as a gripper and an earthworm-inspired robot. Subsequent work used similar valves to demonstrate digital logic circuits for soft robots (*36*) and to generate a soft ring oscillator that produced a continuous oscillatory movement for devices such as a rolling robot and a particle separator (*37*). However, this work has not addressed the challenge of generating more complex, coordinated motions for soft robots with many DoFs, as required to generate responsive gaits for a walking robot.

Nature, however, provides inspiration for how to generate motion from oscillatory circuits. Control circuits known as central pattern generators (CPGs) are used by natural organisms to produce rhythmic movements such as walking, flying, and swimming (*38*). For example, CPGs observed in *Xenopus* tadpoles (*39*) and lampreys (*40*) produce simplified oscillatory movements with minimal feedback. Animals use sensors to regulate their oscillatory gait patterns based on the environment they are navigating (*41*). Examples include stick insects that navigate large gaps by changing their walking speed based on feedback from their antennas (*42*) and cockroaches that use antennas to detect substrate conditions and adapt their walking gait (*43*).

Roboticists have been inspired by pattern-generating biological CPG networks to design robots that can respond to information from their environment (*44*–*46*). For example, decentralized coupled oscillator CPGs observed in caterpillars inspired roboticists to develop a soft-bodied robot that was able to switch between an inching and crawling gait pattern based on tactile sensory information from the environment (*47*). However, previous work on generating robotic gaits based on CPGs has used electric components to generate the patterns.

This work presents pneumatic circuits composed of fluidic control components (*36*, *37*) that are designed to control the gait of a walking robot without electronics (Fig. 1, A to G). Analogous to biological gait control, these circuits generate oscillatory signals and adapt the oscillatory signals in response to sensor input to generate responsive gaits. Our proposed approach for controlling soft systems enables robots to interact with the environment and make decisions based on these interactions without requiring electronics (Movie 1). The innovations that enable this approach are (i) pneumatic circuits composed of a small number of fluidic control components capable of generating gaits for legged locomotion, (ii) a new pneumatic memory element [designed to mimic a double-pole double-throw (DPDT) switch] to enable gait selection, and (iii) an onboard tactile sensor to semiautonomously switch gaits based on input from the environment. Together, these innovations enable simple fluidic circuits for controlling soft-legged robots and represent a step toward developing practical, electronics-free soft robots.

RESULTS

Soft-legged quadruped design

To demonstrate the use of a pneumatic control system on a soft-legged robot, we designed a soft quadruped with three pneumatic chambers per leg [the overall morphology was similar to our previous work (*8*, *9*), Fig. 1]. The four limbs of the robot emanated from the robot body with two perpendicular vertical planes of symmetry. Each limb was angled downward at a 45° angle relative to the horizontal and composed of three parallel, connected pneumatic cylindrical chambers with bellows. When a chamber was pressurized, the limb bent in the opposing direction (Fig. 1E). The three chambers of each limb provided the multiaxis bending required for walking.

Diagonal couplet gait control

The gait for the quadruped was defined by the duration of inflation/deflation for the three chambers of each leg of the robot. Rather than individually addressing all 12 chambers, we simplified the control problem by pairing the similar chambers on the legs diagonally across from one another (Fig. 3B). Here, we refer to the three paired chambers of one diagonal pair as A_1, A_2, and A_3 and the three paired chambers of the other diagonal pair as B_1, B_2, and B_3.

Timed actuation of the paired chambers A_1, then A_2, and then A_3 caused the first pair of legs to rotate in the same direction, causing the robot to take a diagonal step. Similarly, the sequence B_1, then B_2, and then B_3 caused the robot to step in a perpendicular direction (see movie S1).

Reversing the sequence of actuation of the chambers in a leg pair (e.g., A_1, A_3, and A_2) caused the robot to move in the opposite direction (see the "Reversing leg rotation with a 4/2 bistable control valve for omnidirectional locomotion" section). Thus, with linear combinations of forward or reverse steps with the diagonal leg pairs, the robot was able to walk in any direction (see movies S2 and S5). Rotation was also possible by reversing the direction of rotation of one leg in a pair with respect to the other. Thus, a simplified gait control system for omnidirectional locomotion required the diagonal leg pairs to be able to rotate clockwise and counterclockwise. In the following sections, we describe the pneumatic networks that we designed to achieve these rhythmic gait motions with only a single pressure supply line. We also describe how these circuits are used to switch the rotation of the legs in response to user or environmental input.

Rhythmic leg motion with a soft ring oscillator

To control the gait sequences discussed above without electronics, we used soft pneumatic control circuits (*35*–*37*, *48*). The basic rhythmic motion of a pair of legs was generated with a soft ring oscillator (*37*) acting as a pneumatic CPG. The soft ring oscillator propagated continuously with a constant pressure source acting both as signal (i.e., indicating when to oscillate) and source of energy (see the "Soft ring oscillator analysis" section in Methods and Materials for details).

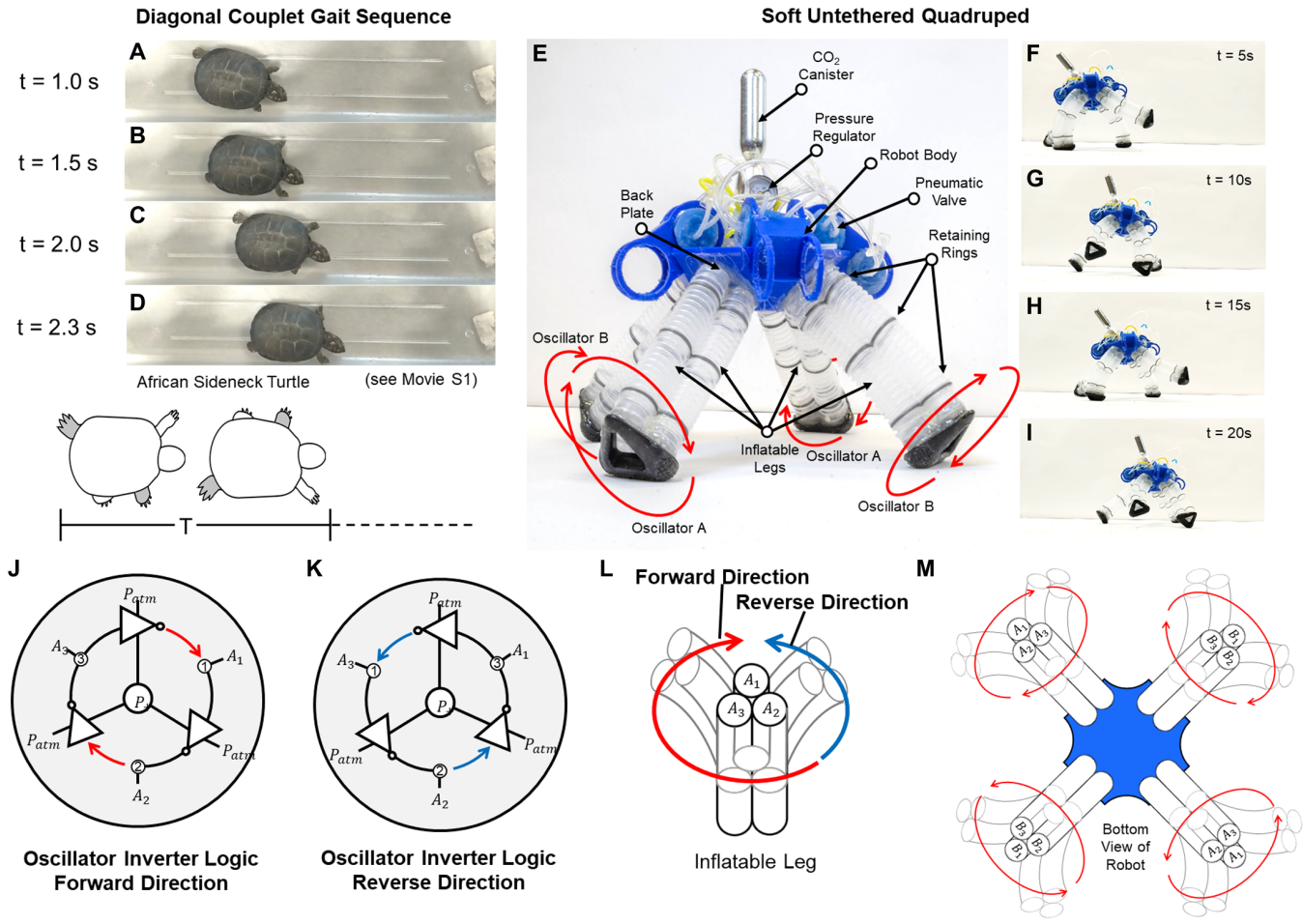

Fig. 1. Soft-legged untethered quadruped robot with a bioinspired gait pattern controlled with an electronics-free pneumatic actuation system. (**A** to **D**) African sideneck turtle exhibiting a diagonal couplet walking gait. (**E**) Image of the untethered quadruped robot with onboard soft valves powered by a pressure-regulated CO_2 canister; key components are labeled, as are the directions of leg motions for forward walking. Pneumatic oscillators are used to control the motions of each diagonal leg pair for forward walking. Each leg of the robot was 173 mm long from base to foot in its neutral state. (**F** to **I**) Sequence of images from a video of the robot walking using only the pressurized CO_2 canister as a source of energy, with two pneumatic oscillator circuits generating rhythmic leg actuation. (**J**) Pneumatic logic circuit for rhythmic leg motion. A constant positive pressure source (P_+) applied to three inverter components causes a high-pressure state to propagate around the circuit, with a delay at each inverter. While the input to one inverter is high, the attached actuator (i.e., A_1, A_2, or A_3) is inflated. This sequence of high-pressure states causes each pair of legs of the robot to rotate in a direction determined by the pneumatic connections. (**K**) By reversing the sequence of activation of the pneumatic oscillator circuit, the attached actuators inflate in a new sequence (A_1, A_3, and A_2), causing (**L**) the legs of the robot to rotate in reverse. (**M**) Schematic bottom view of the robot with the directions of leg motions indicated for forward walking.

Movie 1. Electronics-free air-powered circuits to control the rhythmic movement of a soft legged robot.

To generate rhythmic motion of a pair of legs, we connected one port of each valve of the soft ring oscillator to pneumatic chambers of the legs. One set of paired legs (e.g., chambers A_1, A_2, and A_3) was connected to the nodes of the oscillator circuit (Fig. 2, A to C), which generated pressure in the connected chambers (Fig. 2D). The pressure generated in each chamber during this process was consistent, with an average SD of pressure throughout the cycle of 9.4 kPa (see the "Consistency of pneumatic circuit oscillations" section in the Supplementary Materials).

Simplified pneumatic circuits for controlling two pairs of legs

The soft ring oscillator discussed in the previous section generated continuous oscillatory motion for a single pair of legs. However, the control of a quadruped requires coordination of two sets of diagonally connected pairs of legs to produce a diagonal couplet gait.

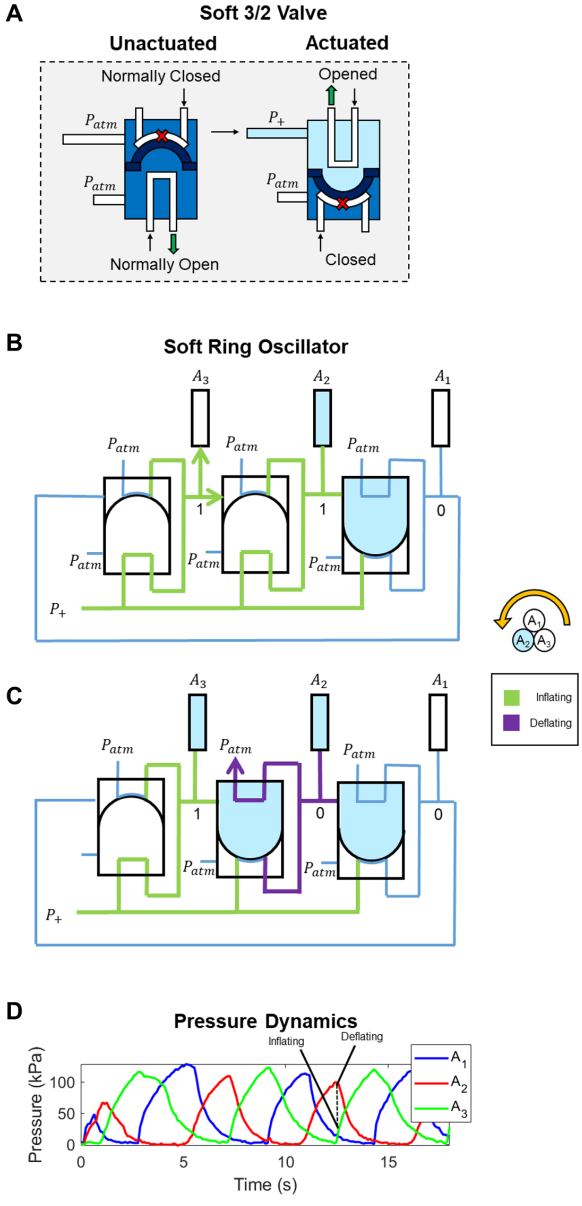

Fig. 2. Soft ring oscillator concept. (**A**) Each of the valves acts as an inverter by switching the normally closed half (top) to open and the normally open half (bottom) to closed. (**B** and **C**) The soft ring oscillator is designed to sequence inflation and deflation of different chambers on the robot (e.g., oscillator *A*: A_1, A_2, and A_3). The soft ring oscillator actuates the chambers in sequence, which results in the limbs rotating in a circle. These schematics depict the moments immediately before (B) and after (C) the pressure in chamber A_3 increases beyond the valve snap-through pressure (P_{st} = 35 kPa). In (B), both A_2 and A_3 are inflating. In (C), once the pressure in $A_3 > P_{st}$, the exhaust for A_2 opens and A_2 begins deflating as depicted. (**D**) Representative plot of the pressure at the three nodes of the oscillator when actuated at 150 kPa. The moments depicted in (B) and (C) are labeled on this plot as inflating and deflating, respectively.

To control both sets of legs, we considered two alternative pneumatic control circuits: a dual-purpose three-valve ring oscillator connected to both leg pairs that we call circuit 1 and a circuit consisting of two three-valve ring oscillators in parallel (six valves to control the oscillation, one valve for phase control) that we call circuit 2. In the following sections, we compare and contrast these options.

Circuit 1: Dual-purpose three-valve ring oscillator circuit

The first circuit for gait control consisted of a ring oscillator composed of three inverter valves (Fig. 3A). This approach actuated both leg pairs simultaneously, but with a phase offset between the leg rotations. We achieved the phase offset by connecting one set of chambers (e.g., A_1, A_2, and A_3 from the first leg pair) to inverters at nodes 1, 2, and 3, respectively, and also connecting the chambers (B_i, B_j, and B_k) to the same inverters but at different node locations. When i = 3, j = 1, and k = 2, this resulted in a phase offset of 120° between the leg rotations, and when i = 2, j = 3, and k = 1, this resulted in a phase offset of 240° (see table in Fig. 3A).

Although the additional capacitance of the chambers from the second pair of legs increased the delay time of each inverter (see the "Soft ring oscillator analysis" section in Methods and Materials), the elimination of four valves (and their corresponding resistances and capacitances) led to a reduced overall period of oscillation. Furthermore, this elimination simplified the control circuit and reduced its mass.

We measured the walking speed for all three phase offsets achievable with this control circuit—0°, 120°, and 240°—and found average robot velocities of −0.005 (s = 0.001), 0.024 (s = 0.007), and 0.014 (s = 0.001) body lengths per second (BL/s), respectively, where s is the sample SD. (Note that with all the legs rotating in unison, all feet stayed in contact with the ground throughout the gait with a little backward motion due to asymmetries in the friction at the feet.) For details on the method of velocity measurement, see the "Robot velocity measurement" section in Materials and Methods. A comparison of these results with the velocity generated by the parallel oscillator circuit (described in the next section) can be found in Fig. 3C.

Circuit 2: Parallel oscillator circuit

Tortoises with a diagonal couplet gait pattern have about a 180° phase offset between the periodic forces exerted by the diagonal pairs of feet (*49*). It is hypothesized that tortoises have adopted this gait to minimize metabolic cost (*50*, *51*). In our experiments with diagonal couplet gaits with 120° or 240° phase offsets, we observed interference of one couplet with the other that reduced the overall speed of locomotion. The possibility of improved locomotion performance with a 180° phase offset between the diagonal couplets motivated us to design and test a second gait control circuit.

Circuit 2 consisted of two ring oscillators acting in parallel, each of which controlled one pair of legs (one couplet). To tune the phase offset between the two oscillators, we introduced an additional inverter valve to control a time delay element. This time delay element was designed to delay the second oscillator only once upon initiation of the circuit (Fig. 3, D to F). After initially changing state, the soft valve bypassed the resistor, so the resistor would no longer affect the period of oscillation. Thus, after the initial delay, the second oscillator produced the same actuation as its parallel twin, except with a phase offset between the two (plus any variations due to imperfect fabrication). This approach provided finer control of the phase offset between the motions of the diagonal pairs of legs but required a total of seven valves (six valves for oscillator control and one valve for phase control).

Comparison of pneumatic control circuits

To validate the hypothesized improved performance of the locomotion gait produced by circuit 2, we measured the speed of the robot with the phase tuned to about 180° (see the "Robot velocity measurement" section in Materials and Methods). For gait cycles in which the

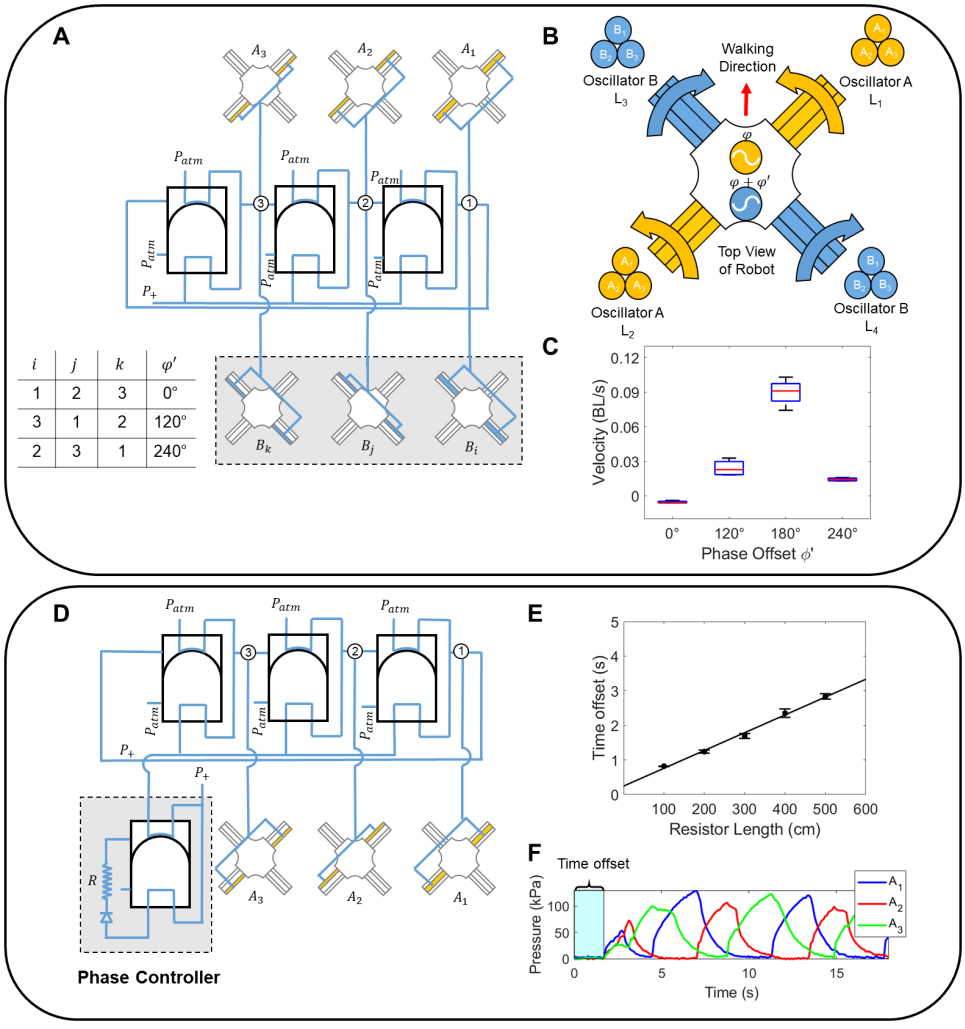

i	j	k	φ'
1	2	3	0°
3	1	2	120°
2	3	1	240°

Fig. 3. Simple circuits for generating a diagonal couplet gait. (**A**) The dual-purpose three-valve ring oscillator circuit (labeled as circuit 1) controlled the pressure in 12 chambers with four chambers (two mirrored pairs) connected to each inverter for a phase offset of 0°, 120°, or 240° between the rotation of each diagonal leg pair (depending on the positions of the second pair of chambers relative to the first). (**B**) Schematic of the quadruped robot controlled by oscillator A and oscillator B when oscillator B has a phase offset of φ′. (**C**) Box plot depicting the velocity of the robot for four different phase offsets. The 0°, 120°, and 240° phase offsets were controlled with circuit 1, and the 180° phase offset was controlled by circuit 2. (**D**) The parallel oscillator circuit (circuit 2) consisted of two oscillators controlling the two leg pairs in parallel. One of the oscillators was delayed by a phase controller (pictured here), and the other was not (not pictured), resulting in a one-time delay of one oscillator with respect to the other upon activation of both circuits. (**E**) The delay was adjusted by changing the resistance of an element *R* (i.e., the length and inner diameter of a section of tubing) connected to an inverter so that it only delayed the circuit once at the initiation of oscillation. (**F**) Representative measurement of the pressure in the three chambers of the delayed oscillator. The time offset delayed the initiation of the second oscillator (shaded region), effectively controlling the phase between two oscillators.

phase offset between the legs was about 180°, we measured a walking speed of 0.090 (s = 0.012) BL/s (see Fig. 3C). When comparing this value to those for measured for circuit 1 with fixed phase offsets of 0°, 120°, and 240°, we found at least a 270% increase in the speed of the robot with circuit 2, justifying the additional four valves required. Note that this speed increase was in spite of the increased mass of circuit 2 (~112 g) due to the four extra valves. On the basis of our untethered experiments with varying payload (see the "Untethered operation" section and fig. S3), we would expect a 10% decrease in the speed of the robot due to the effects of this added mass alone (assuming a linear effect of payload).

Although the negative effects of the additional weight of the valves of circuit 2 were outweighed by the improved efficiency of the gait, our testing revealed a more practical concern: The additional valves introduced more potential points of failure. This consideration was especially important for our case of laboratory-manufactured components, which had limited life spans. Thus, to minimize the risk of failure, we chose to use circuit 1 for the majority of our experiments, despite the reduced speed.

Reversing leg rotation with a 4/2 bistable control valve for omnidirectional locomotion

The soft ring oscillator circuits described above actuated the pneumatic chambers of the legs in continuous, cyclical patterns (with various phase offsets between the diagonal couplets). However, to change the walking direction, a more complex circuit was required to reverse the sequence of actuation of the chambers. To achieve this direction reversal with a reduced number of additional components, we designed a component to selectively switch the connections between two of the mirrored pairs of chambers and two of the ring oscillator valves, resulting in a reversed sequence. (Note that this reversal was simplified by the fact that the robot had only three pneumatic chambers per leg. For a leg with more pneumatic chambers, this reversal would have required a more complex circuit.)

We switched the connections between the oscillator and the pneumatic chambers using a soft 4/2 bistable control valve that is analogous to a latching DPDT switch (Fig. 4A). This valve controlled the flow between four ports by switching between two different states [corresponding to counterclockwise or clockwise rotation of the limbs; Fig. 4, B and C, respectively]. Our design switched the state of an elastomeric membrane similar to that used in the 3/2 soft valves of the ring oscillator (see Fig. 2), except with two (rather than one) fluid lines connected to either side of the membrane. As a result, the sequence of chamber pressurization reversed when pressure was applied to switch the state of the 4/2 valve (either manually or with a fluid; Fig. 4D). Because the membrane was bistable, the valve did not require continuous pressure to remain in a state.

The 4/2 valve was partially enabled by an innovation in our soft valve design as compared with previous soft valves used to actuate soft robots (*35*–*37*): We found that, by adhering the tubes directly to

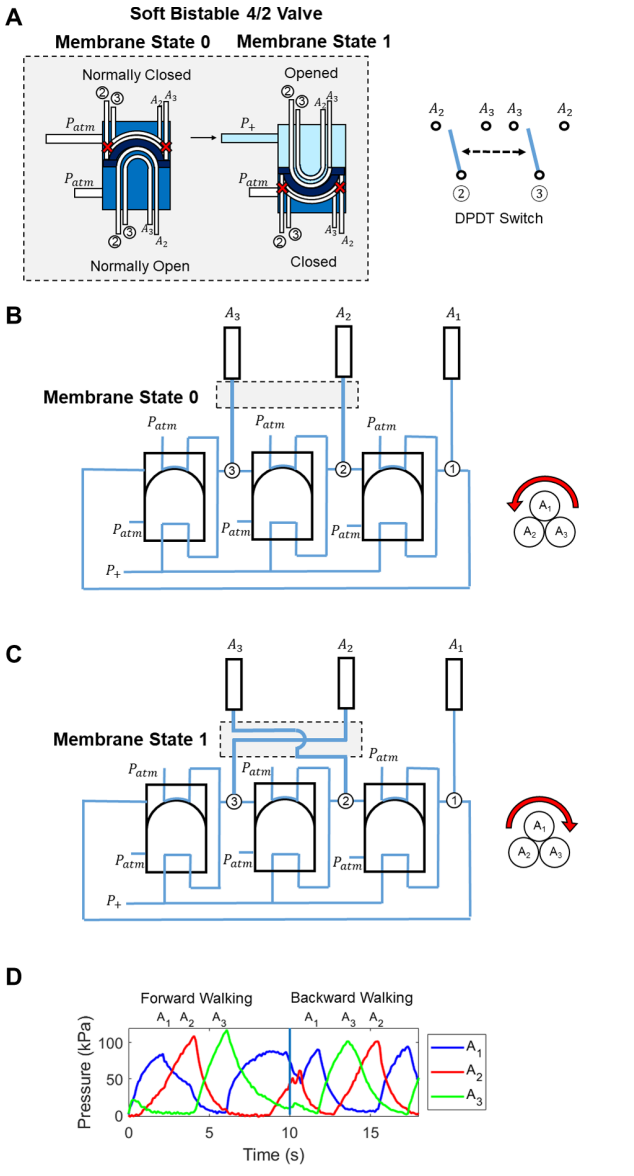

Fig. 4. Soft bistable 4/2 valve for switching gaits. (**A**) Operation of the 4/2 valve acting as a latching DPDT switch. The valve switches the direction of rotation of the limbs between (**B**) counterclockwise and (**C**) clockwise. (**D**) Representative plot of the pressure in the three chambers A_1, A_2, and A_3 before and after the controlling 4/2 valve is switched (vertical line at 10 s).

the membrane, they could be kinked (closed) in one membrane state and opened in the other (see Fig. 4). This approach allowed us to simply adhere both tubes next to one another for the 4/2 valve. See the "Soft valve fabrication" section in Materials and Methods for fabrication details.

The bistable valves allowed selection of the direction of rotation of each pair of legs. Thus, we used two 4/2 bistable control valves (one for each leg pair) to control the translational walking directions of the robot (Fig. 5A). Two more 4/2 valves (e.g., one per leg, to individually control the direction of rotation of each leg) could be used to control either clockwise or counterclockwise rotation (Fig. 5B), which is left for future work. The mapping between the 4/2 valve states and the motions of the robot are shown in the tables in Fig. 5.

Tethered control of omnidirectional locomotion

To test control of omnidirectional locomotion, we developed a manual controller to control two 4/2 valves (Fig. 6, A to C, and movie S2). Each position on the manual controller corresponded with half of a 4/2 valve to keep tube routing underneath the controller. This required us to press one of the two positions corresponding to the full 4/2 valve to control the walking direction of the robot (pressing both simultaneously would result in an undefined gait). We sequentially commanded the robot to walk forward, left, backward, and then right by changing the corresponding valve states with the manual controller. Aside from this input, the robot required only a constant source of pressure to generate the appropriate gaits. We demonstrated omnidirectional control (Fig. 5 and movie S2) using the dual-purpose three-valve ring oscillator circuit. Although this circuit resulted in slower gaits, it was simpler and lighter than the alternatives, which each required seven valves. As a demonstration of the use of omnidirectional locomotion for obstacle avoidance, we controlled the diagonal motion generated by one oscillator with forward movement generated by both oscillators to navigate around an obstacle (Fig. 6, D to F, and movie S4).

The motion of the robot was quasi-static (no ballistic phase). Thus, when one pair of legs rotated, the robot leaned on one of the limbs of the opposite diagonal pair to remain stable. As a result, on the basis of tracked data of six steps from movie S1, the top of the feet lifted an average of 150.93 mm (s = 27.44 mm), which is 72% of the robot height. The ability of the robot to lift its feet this high off the ground could enable the robot to navigate over a variety of obstacles. We leave further investigation of navigating over obstacles to future work.

Tactile sensor

We designed a soft sensor to semiautonomously trigger a reversal of the walking gait upon contact (Fig. 7 and movie S5). The sensor was composed of an elastomeric membrane connected by a fluidic transmission to a 4/2 bistable control valve. When an object contacted the sensor, the membrane pushed on the enclosed transmission fluid (water) to immediately switch the state of a connected 4/2 control valve, resulting in a reversal of the direction of motion of the robot (see the previous section). This computation was done onboard the robot without any electrical components. To increase the sensitivity of the sensor to external contact, we prepressurized the transmission fluid until the connected 4/2 valve was near the point of instability but still stable (the fluid was initially pressurized to less than P_{st} for the bistable valve to remain in the initial state).

Untethered operation

We demonstrated untethered walking of the robot by powering it with a disposable CO_2 canister and a pressure regulator (Fig. 1, A to G). We tested the robot walking with the CO_2 regulated to 140 kPa. The smaller 57-g CO_2 canisters provided ~45 s of operation and the larger 306-g canister provided ~4 min at this operating pressure. We used circuit 1 for each of the demonstrations of the untethered robot.

Although the larger canister provided a longer operating time, the added weight of the larger canister and regulator (666 g or 170% of the weight of the robot) negatively affected the speed of the robot, causing it to walk 42% slower than when carrying the smaller canister and regulator (194 g; see fig. S3).

In addition, we measured the mass of compressed gas used per unit distance traveled by the robot when walking over a 30-s interval of the gait by weighing the canisters before and after walking.

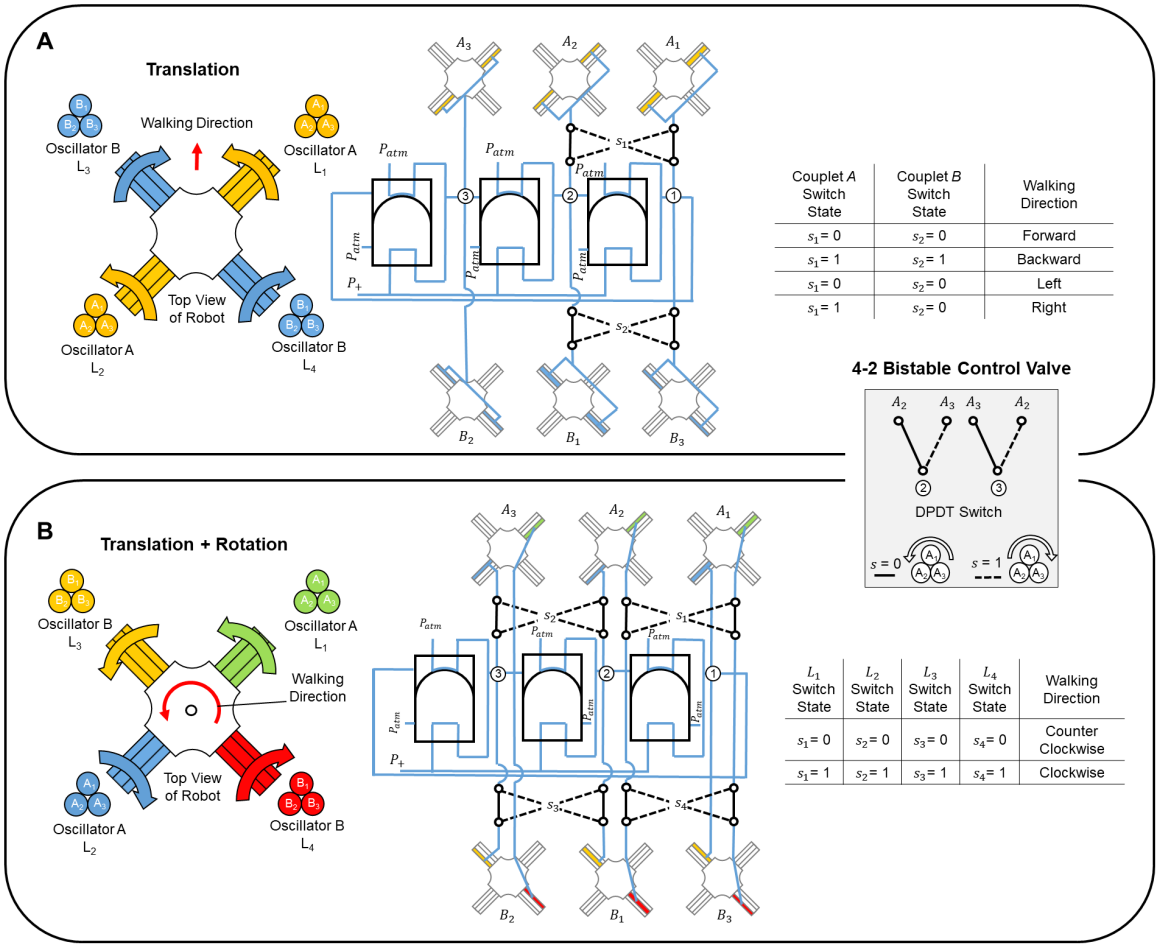

Fig. 5. Omnidirectional control of the walking direction of the robot with 4/2 valves. (**A**) The output sequences of a three-valve ring oscillator circuit are controlled by the states of the two 4/2 valves. The states of the valves control the direction of rotation of the two diagonal leg pairs. We connected the 4/2 valve between two of the chambers to switch the chamber order for the soft ring oscillator sequence. The robot can translate in four directions based on the states of the two 4/2 valves. (**B**) By adding a 4/2 valve to the outputs corresponding to each leg, the robot can rotate clockwise or counterclockwise in addition to translating in any direction.

While carrying the large canister, the robot used 1.7× the mass of compressed gas per unit distance traveled as compared with while carrying the small canister. Thus, the smaller CO_2 canister and regulator is a more efficient power source for the robot during untethered operation but resulted in a robot with a reduced operation time (45 s versus 4 min).

Even while controlled with a completely pneumatic circuit and carrying its power source, the robot presented here demonstrated a comparable top speed (0.09 BL/s) to our previous, tethered, and soft-legged robot controlled by electromechanical components (0.13 BL/s) (*8*, *9*).

DISCUSSION

Soft, pneumatically actuated valves are inexpensive, lightweight, and easy to manufacture as compared with the electromechanical valves commonly used to control soft robots. With appropriate design, these components can be combined to create sophisticated fluidic circuits that can control the gaits of legged robots without any electronics. In this work, we demonstrated the use of such fluidic circuits to control the omnidirectional locomotion of a soft-legged robot to navigate around obstacles. These circuits used a soft ring oscillator composed of soft valves to generate rhythmic motions, which were acted on by additional control elements to adjust the walking gaits autonomously or based on manual input.

The properties of biological CPGs provide benefits for walking gaits because they enable animals to generate stable rhythmic movements using minimal control inputs (i.e., minimal descending locomotor commands) (*38*, *52*). In particular, (i) the neurons in CPG networks produce signals that generate oscillatory motions (gaits), (ii) these oscillatory signals are robust to disturbances, and (iii) sensor inputs act on these signals to adjust the gaits in response to interactions with the environment. In this work, we have demonstrated each of these properties with our experimental soft robotic system. First, each of the pneumatic circuits presented in this work used a single pneumatic source to generate oscillatory motion, which reduced the number of components—and hence the weight—of the robotic system. Second, when perturbed (by temporarily changing the pressure in the pneumatic circuit), the circuits returned to their rhythmic oscillation within one cycle (see the "Robustness of pneumatic circuit to pressure variations" section in the Supplementary Materials). Third, the pneumatic logic components and sensors

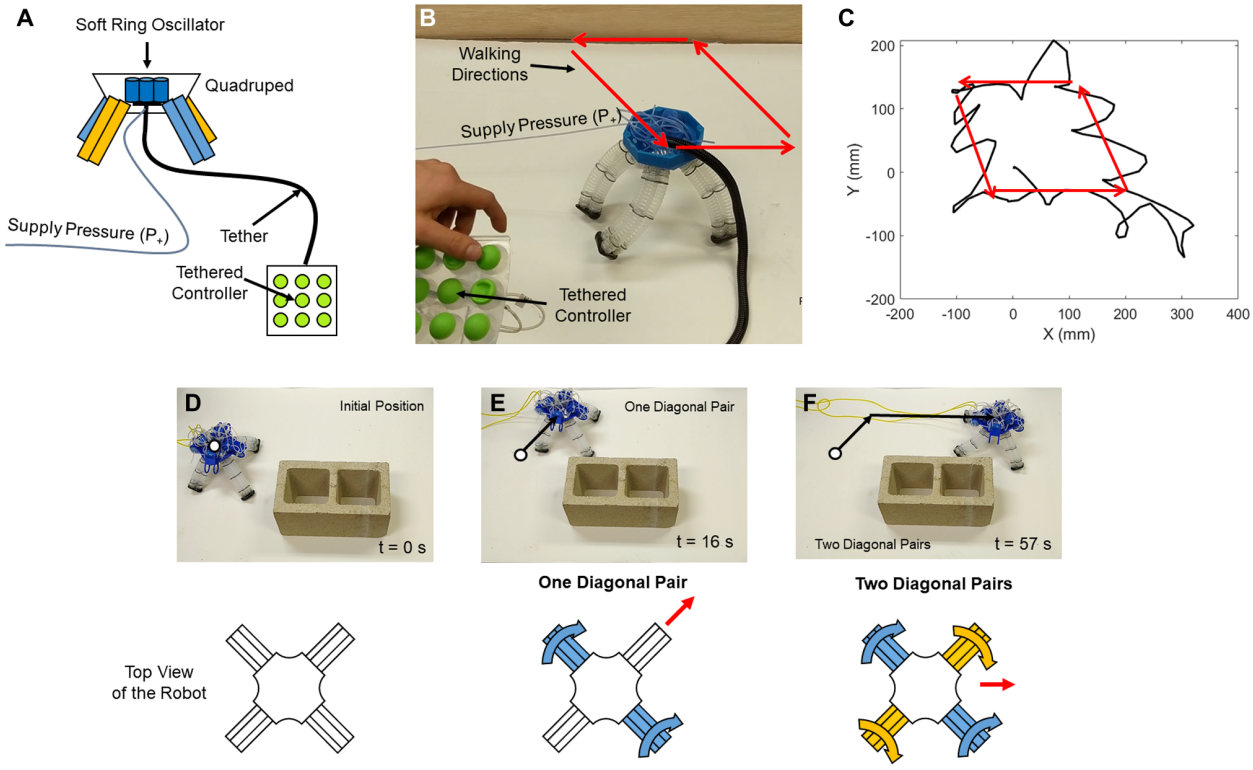

Fig. 6. Tethered control of the quadruped robot. (**A**) Schematic of the robot, with a single pressure supply line, tethered to a manual controller. (**B**) Image from demonstration of the robot walking forward, left, backward, and then right in sequence, with commanded directions indicated. (**C**) *X-Y* position of a single point on the robot body during the experiment (see movie S2) tracked from the video with motion tracking software. (**D** to **F**) Images of demonstration of manually controlled obstacle avoidance by first walking diagonally using one diagonal pair of legs and then walking forward with both diagonal pairs, with associated schematics indicating the actuation of the legs.

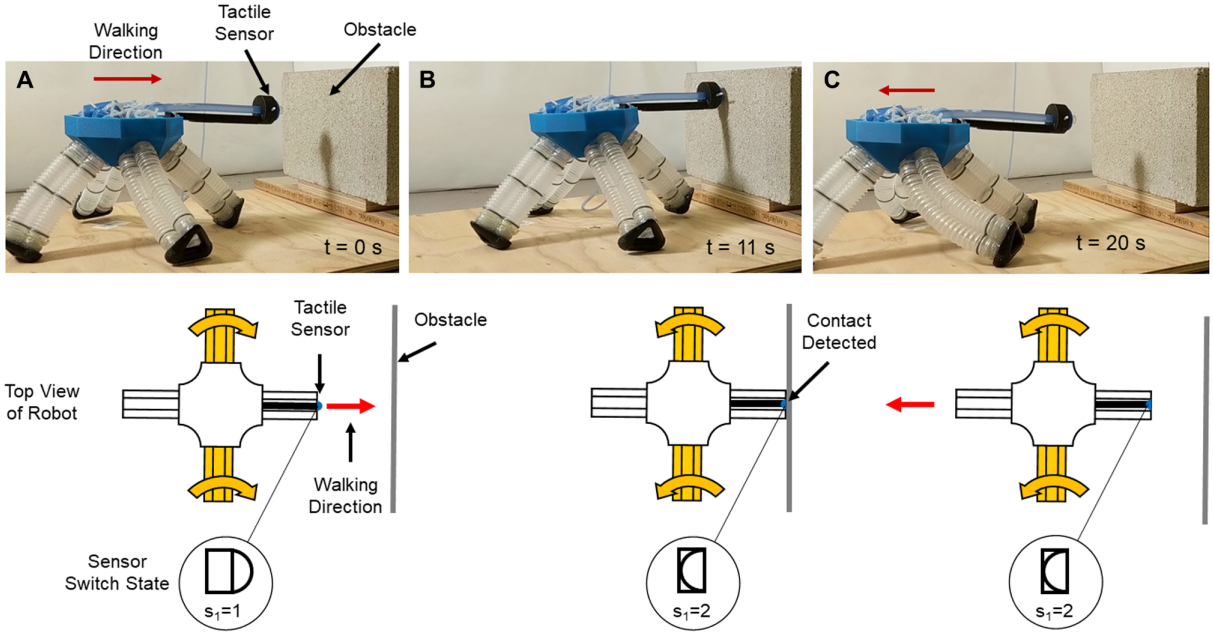

Fig. 7. Sensor input for autonomous gait reversal. Contact with the wall switches the walking direction of the robot by switching the state of a soft sensor that is connected to a 4/2 bistable valve. (**A**) The pneumatic control circuit powered by a constant pressure source actuated one diagonal pair of legs causing the robot to walk toward a wall. (B) When the soft sensor contacted the wall, the soft sensor switched state, and (**C**) the robot began walking in the opposite direction.

presented in this work allowed the robot to adjust its stable rhythmic pattern based on information from the external world.

With the approach described here, it is possible to modulate the frequency and amplitude of the walking gaits (and hence the speed and foot clearance of the walking robot) based on the design of the pneumatic components (e.g., the dimensions of the membranes of the valves). Previous work analyzed (*53*) and experimentally characterized (*37*) the effect of membrane dimensions on their snap-through and snap-back pressures. In this work, we have described the relationships between the snap-through and snap-back pressures required to choose a set of membrane parameters appropriate for our walking robot. Future work could investigate ways to adjust these parameters (e.g., switching between valves with different membrane dimensions) to adjust the amplitude and frequency of limb oscillation during operation.

Circuit 2 was designed with a delay element to offset the phase of one oscillator relative to another. Ideally, this phase should not shift over time. However, due to our manufacturing method and the materials used, we observed variabilities between the pneumatic parameters of the valves and the chambers of the robot, as well as temporal variation in these parameters (see fig. S1). These inconsistencies did not have a large impact on the gait for the time frames we tested. However, future work could consider phase-locking circuits designs that can be used to prevent a shift over time in the phase between the leg pairs due to manufacturing variabilities. Circuit 1 had the advantage of avoiding this problem.

The physical size of the elements of the pneumatic circuit depended on the requirements placed on the circuit—i.e., the pneumatic elements were designed to work within the operating pressures of the soft robot, and the pneumatic elements were required to transmit sufficient fluid to actuate the robot. As a result, the elements added considerable mass and volume to the system, both of which place a limit on the performance of an untethered walking robot. These challenges are exacerbated by the increase in complexity of the circuit required to increase the autonomy of the system. Approaches to reduce the mass and volume of the pneumatic circuits are needed, perhaps by separating the pneumatic system into "power" and "control" circuits as is typically done with electronics.

This work could be extended to apply to robots with more/fewer limbs or limbs with a different number of DoFs. The number of DoFs for the oscillatory movement scales linearly with the number of valves as long as the number of chambers is odd (e.g., oscillating three chambers requires three valves, but oscillating four chambers requires five valves). However, reversing sequences of more than three chambers requires more 4/2 bistable valves. By inspection, we find that for n chambers on each leg (when n is greater than 1 and odd), there needs to be $\frac{n-1}{2}$ bistable valves to change the direction of rotation of the legs.

Future work could also investigate increasing the mobility of soft walking robots. Potential avenues of research include autonomous object traversal and the navigation of natural terrains. These feats would likely require a more sophisticated network of sensors and a correspondingly more complex pneumatic control system.

Overall, the integration of soft pneumatic control circuits into the body of the robot is a step toward autonomous, electronics-free, and mobile soft robotic systems. Inspired by animals with simple nervous systems that are able to produce coordinated oscillatory movements regulated by sensor feedback (*39*, *40*), this work has demonstrated a pneumatically powered and controlled soft robot to generate complex locomotion without electronics. This approach could lead to robots useful for a variety of applications, including operating in environments sensitive to spark ignition (e.g., in underground mines) or that do not allow metal (e.g., in an operating magnetic resonance imaging machine) or for the mass production of simple, inexpensive autonomous systems (e.g., for cleaning robots or for entertainment). (For further discussion of potential applications, see the "Considerations for future applications" section in the Supplementary Materials.)

MATERIALS AND METHODS

Soft robot fabrication

To manufacture the soft-legged quadruped, we used commercially available polyvinyl chloride cylindrical bellows (Corr-A-Flex Tubing, Teleflex Inc.) for the pneumatic chambers due to their extrinsic compliance (to allow bending) combined with the intrinsic stiffness of the material (to permit large internal pressures). As a result, we were able to actuate the robot with a maximum internal pressure of 170 kPa [compared with 110-kPa pressure for our previous, three-dimensional (3D) printed legs (*8*, *9*)]. The sections of tubing were held together with retaining rings. The robot body and retaining rings were 3D printed out of polylactic acid (PLA; MakerBot Replicator 2, Stratasys Inc.). We used a commercial multimaterial 3D printer (Connex 3, Stratasys Inc.) to print the feet of the robot of a soft material (TangoBlack+) for traction, as well as rigid back plates to mount the legs to the body of the robot (VeroClear).

Soft valve fabrication

The valves comprised a cylindrical body, two caps, and tubing. The body of the soft valves and caps was molded out of a soft polymer (MoldStar 30, Smooth-On Inc.). The polymer was poured into a 3D printed mold made of PLA (MakerBot Replicator 2). The caps closed off the normally closed and normally open cavities of the valve. We used a silicone adhesive (Sil-Poxy) to adhere the caps of the valve to the cylindrical body. Tubes were fed through the side walls of the cylindrical body and the caps to create the inlet, exhaust, and opened/closed airways (see Fig. 2). Please refer to the Supplementary Materials for more details.

Control valve characterization

We measured the snap-through and snap-back pressures for an individual 3/2 valve, which resulted in an average of 35 kPa (s = 3 kPa) and 20 kPa (s = 2 kPa), respectively. We fit the pressure dynamics to an exponential function (solution to Eq. 1) and found a time constant ($\tau = RC$) of 1.32 s. We measured the snap-through pressure for an individual bistable 4/2 valve (including tubing on both sides) to be 35 kPa (s = 5 kPa).

Soft ring oscillator analysis

The soft ring oscillator was formed by connecting three three-port and two-state (3/2) control valves in series, where the output from one valve served as the input to the next valve (Fig. 2, A to C). Each of the soft valves acted as an inverter (i.e., a NOT logic gate) with a time delay; thus, the soft valves switched the state of each connected chamber from a high (inflated) state to a low (deflated) state, or vice versa. The valves regulated flow by closing and opening channels using a snap-through instability in a hemispherical elastomeric membrane. The valves switched between one of two states whether pressure was applied to the surface of the membrane.

The pneumatic soft ring oscillator can be modeled on the basis of analogous electrical components (*37*), leading to the following relationships for the resistance, capacitance, and pressure dynamics of the valves

$$\frac{dP}{dt} = \frac{1}{RC}(P_i - P) \quad (1)$$

$$R = R_{tubing} + R_{inverter} \quad (2)$$

$$C = C_{chamber} + C_{inverter} \quad (3)$$

$$R_{tubing} = \frac{128\mu L}{\pi\rho D^4} \quad (4)$$

$$C_{chamber} = \frac{V_0 M}{R_u T} \quad (5)$$

where μ is the dynamic viscosity of air, L is the length of the tubing, ρ is the density of air, D is the inner diameter of the tubing, $C_{inverter}$ is capacitance of the inverter, $R_{inverter}$ is resistance of the inverter, R_{tube} is the resistance of added tubing, V_0 is the volume of air in the reservoir, M is the molar mass of the air, R_u is the universal gas constant, T is the temperature of the air, and P_i can either be P_+ (supply pressure) on inflation or P_{atm} on deflation.

The time delay propagated through each valve t_p was determined on the basis of the two states of the membrane in the valve

$$t_p = RC\left[\ln\left(\frac{P_{atm} - P_+}{P_{st} - P_+}\right) + \ln\left(\frac{P_+ - P_{atm}}{P_{sb} - P_{atm}}\right)\right] \quad (6)$$

where P_{st} is the snap-through pressure of the membrane, P_{sb} is the snap-back pressure of the membrane, and the supply pressure is P_+. If the tubing, chambers, and valves in the soft ring oscillator are the same, the period of oscillation is $T = nt_p$, where n is the total number of valves. The values of R and C can be tuned to adjust the time it takes for pressure to propagate through each valve; hence, R and C can be used to adjust the period and timing of a soft ring oscillator.

Soft ring oscillator characterization

We measured the pressure in the oscillator at the nodes connected to one set of diagonally connected legs and processed the data with a 10-point moving average sampled at 40 Hz for the case of free oscillation (Fig. 2D). The average period for one complete cycle of the soft ring oscillator actuated at 150 kPa was 8.13 s (s = 0.12 s). The nodal pressures were measured with pressure sensors (Honeywell International Inc., 100PGAA5). The period between the peak pressures measured in each sequential node was 2.73 s on average (s = 0.12 s). Differences between the pressure signals were due to slight variations in the fabrication of each valve.

For a soft ring oscillator formed of bistable valves, a high-frequency spike occurred in the pressure when it reached the critical snap-back and snap-through pressures of the membrane (*37*). In our oscillator, the pairs of limbs of the robot stored large volumes of air (i.e., had high capacitance), thus effectively acted as low-pass filters, filtering these high-frequency pressure changes (Fig. 2D).

Setting the phase delay of the parallel oscillator control circuit

The time offset for the parallel oscillator circuit was controlled by adjusting the length of tubing of the resistor. The length of tubing changed the time delay of the second oscillator with respect to the first in the parallel oscillator circuit (see the "Circuit 2: Parallel oscillator circuit" section in Results). We measured the time delay in the ring oscillator circuit using different tube lengths (Fig. 3E). To determine the time offset, we measured the pressure before and after the phase control elements as we applied a step input pressure. We performed five experiments for each resistor length and fit the data points to a linear trend line. An increase in the length of the tubing corresponded with a linear increase in the phase offset. This is consistent with our model, which predicts that the time delay of a valve varies linearly with its resistance R (Eq. 6). We used tubing with a 0.3 mm inner diameter that was looped to keep the resistor in a small form factor. We looped the tubing eight times for each trial to control for the effect of the number of loops of tubing on the fluidic resistance. Each length of tubing was tested three times at a constant applied pressure of 155 kPa. The capacitance of the additional valve and tubing connecting the phase controller to the circuit also contributed to the time offset (we assumed that this was constant for each trial, i.e., that the capacitance change due to the change in the length of the looped tubing was negligible). We used an approach similar to that used to characterize the pressure in the soft ring oscillator (see the previous section) to measure the pressure in the nodes of the oscillator with a phase delay component (Fig. 3F).

Characterization of oscillation reversal with a 4/2 valve

We used an approach similar to the one used to characterize the pressure in the soft ring oscillator (see the "Soft ring oscillator characterization" section) to measure the pressure in the nodes of the oscillator before and after a 4/2 valve was used to switch the output sequence (Fig. 4D). The timing within the oscillation cycle in which the 4/2 valve switched state determined how the pressure responded (i.e., pressure stored in the chambers, tubing, and valves was either released or reused after the switching occurred). Although variable, the time delay during the transition was small (<1 s) relative to the time scale of the oscillation period. The experiments for switching the direction of the robot were performed using circuit 1; however, because the soft ring oscillator circuit was identical to those used in circuit 2, the direction reversal would work in the same way in both cases. It should be noted, however, that the simultaneous reversal of the two oscillating circuits could lead to variations in the phase offset between these circuits. We leave further investigation of this challenge to future work.

Controller fabrication

A manual controller was manufactured to control the walking direction of the robot. The controller was manufactured from an array of bistable elastomeric hemispheres from an ice tray (Zing Pop-Out Ice Cube Tray, Robinson Home Products Inc.). Each position on the controller was designed to behave in the same way as half of a 4/2 control valve. There were two tubes beneath each position on the controller that kinked when each of the membranes on the controller were pressed. The tubes routed beneath each of the membranes were routed as shown in Fig. 5A.

Robot velocity measurement

We measured the velocity of the robot by tracking the movement of the robot body during multiple gait cycles. We actuated the robot with a set gait sequence and used the body of the robot and leg of the robot as visual markers to measure the displacement of the robot for each cycle. We recorded videos for each gait and tracked the position of the body using an open-source video analysis software [Tracker (*54*)].

SUPPLEMENTARY MATERIALS

robotics.sciencemag.org/cgi/content/full/6/51/eaay2627/DC1
Supplementary Text
Fig. S1. Consistency of the soft ring oscillator.
Fig. S2. Motion of the foot of the robot when the pressure in the pneumatic controller is perturbed.
Fig. S3. Comparison of the speed of the robot while carrying the small (left) and large (right) CO_2 canisters and regulators.
Table S1. List of .stl files.
Data S1. Archive of .stl files (.zip format).
Movie S1. Video of the African sideneck turtle exhibiting a diagonal couplet walking gait.
Movie S2. Video of omnidirectional locomotion, controlled by the four states of two DPDT soft pneumatic switches.
Movie S3. Video of robot walking untethered, powered by a pressurized CO2 canister fitted with a pressure regulator.
Movie S4. Demonstration of the robot navigating around an obstacle, with manual switching from a single leg pair diagonal gait to a diagonal couplet walking gait, controlled by a dual-purpose three-valve ring oscillator, accelerated 4×.
Movie S5. Video of the electronics-free robot autonomously avoiding an obstacle.

REFERENCES AND NOTES

1. D. Rus, M. T. Tolley, Design, fabrication and control of soft robots. *Nature* **521**, 467–475 (2015).
2. R. F. Shepherd, F. Ilievski, W. Choi, S. A. Morin, A. A. Stokes, A. D. Mazzeo, X. Chen, M. Wang, G. M. Whitesides, Multigait soft robot. *Proc. Natl. Acad. Sci. U.S.A.* **108**, 20400–20403 (2011).
3. A. D. Marchese, C. D. Onal, D. Rus, Autonomous soft robotic fish capable of escape maneuvers using fluidic elastomer actuators. *Soft Robot.* **1**, 75–87 (2014).
4. T. Umedachi, V. Vikas, B. Trimmer, Softworms: The design and control of non-pneumatic, 3D-printed, deformable robots. *Bioinspir. Biomim.* **11**, 025001 (2016).
5. A. O'Halloran, F. O'malley, P. McHugh, A review on dielectric elastomer actuators, technology, applications, and challenges. *J. Appl. Phys.* **104**, 071101 (2008).
6. R. S. Kularatne, H. Kim, J. M. Boothby, T. H. Ware, Liquid crystal elastomer actuators: Synthesis, alignment, and applications. *J Polym Sci B* **55**, 395–411 (2017).
7. P. Polygerinos, N. Correll, S. A. Morin, B. Mosadegh, C. D. Onal, K. Petersen, M. Cianchetti, M. T. Tolley, R. F. Shepherd, Soft robotics: Review of fluid-driven intrinsically soft devices; manufacturing, sensing, control, and applications in human-robot interaction. *Adv. Eng. Mater.* **19**, 1700016 (2017).
8. D. Drotman, S. Jadhav, M. Karimi, P. deZonia, M. T. Tolley, 3D printed soft actuators for a legged robot capable of navigating unstructured terrain, in *2017 IEEE International Conference on Robotics and Automation (ICRA)* (IEEE, Singapore, 29 May to 3 June 2017).
9. D. Drotman, M. Ishida, S. Jadhav, M. T. Tolley, Application-driven design of soft, 3-d printed, pneumatic actuators with bellows. *IEEE/ASME Trans. Mechatron.* **24**, 78–87 (2019).
10. M. Ishida, D. Drotman, B. Shih, M. Hermes, M. Luhar, M. T. Tolley, Morphing structure for changing hydrodynamic characteristics of a soft underwater walking robot. *IEEE Robot. Autom. Lett.* **4**, 4163–4169 (2019).
11. M. T. Tolley, R. F. Shepherd, B. Mosadegh, K. C. Galloway, M. Wehner, M. Karpelson, R. J. Wood, G. M. Whitesides, A resilient, untethered soft robot. *Soft Robot.* **1**, 213–223 (2014).
12. J. Zou, Y. Lin, C. Ji, H. Yang, A reconfigurable omnidirectional soft robot based on caterpillar locomotion. *Soft Robot.* **5**, 164–174 (2018).
13. C. D. Onal, X. Chen, G. M. Whitesides, D. Rus, *Robotics Research* (Springer, 2017), pp. 525–540.
14. C. D. Onal, D. Rus, Autonomous undulatory serpentine locomotion utilizing body dynamics of a fluidic soft robot. *Bioinspir. Biomim.* **8**, 026003 (2013).
15. R. K. Katzschmann, A. D. Marchese, D. Rus, *Experimental Robotics* (Springer, 2016), pp. 405–420.
16. R. K. Katzschmann, J. DelPreto, R. MacCurdy, D. Rus, Exploration of underwater life with an acoustically controlled soft robotic fish. *Sci. Robot.* **3**, eaar3449 (2018).
17. A. A. Calderón, J. C. Ugalde, J. C. Zagal, N. O. Pérez-Arancibia, Design, fabrication and control of a multi-material-multi-actuator soft robot inspired by burrowing worms, in *2016 IEEE International Conference on Robotics and Biomimetics (ROBIO)* (IEEE, Qingdao, China, 3 to 7 December 2016), pp. 31–38.
18. D. Ortiz, N. Gravish, M. T. Tolley, Soft robot actuation strategies for locomotion in granular substrates. *IEEE Robot. Autom. Lett.* **4**, 2630–2636 (2019).
19. N. W. Bartlett, M. T. Tolley, J. T. B. Overvelde, J. C. Weaver, B. Mosadegh, K. Bertoldi, G. M. Whitesides, R. J. Wood, A 3D-printed, functionally graded soft robot powered by combustion. *Science* **349**, 161–165 (2015).
20. D. P. Holland, E. J. Park, P. Polygerinos, G. J. Bennett, C. J. Walsh, The soft robotics toolkit: Shared resources for research and design. *Soft Robot.* **1**, 224–230 (2014).
21. A. D. Marchese, K. Komorowski, C. D. Onal, D. Rus, Design and control of a soft and continuously deformable 2d robotic manipulation system, in *2014 IEEE International Conference on Robotics and Automation (ICRA)* (IEEE, Hong Kong, China, 31 May to 7 June 2014), pp. 2189–2196.
22. T. Kalisky, Y. Wang, B. Shih, D. Drotman, S. Jadhav, E. Aronoff-Spencer, M. T. Tolley, Differential pressure control of 3D printed soft fluidic actuators, in *2017 IEEE/RSJ International Conference on Intelligent Robots and Systems (IROS)* (IEEE, Vancouver, BC, Canad, 24 to 28 September 2017), pp. 6207–6213.
23. M. A. Unger, H.-P. Chou, T. Thorsen, A. Scherer, S. R. Quake, Monolithic microfabricated valves and pumps by multilayer soft lithography. *Science* **288**, 113–116 (2000).
24. B. Mosadegh, A. D. Mazzeo, R. F. Shepherd, S. A. Morin, U. Gupta, I. Z. Sani, D. Lai, S. Takayama, G. M. Whitesides, Control of soft machines using actuators operated by a Braille display. *Lab Chip* **14**, 189–199 (2014).
25. N. W. Bartlett, K. P. Becker, R. J. Wood, A fluidic demultiplexer for controlling large arrays of soft actuators. *Soft Matter* **16**, 5871 (2020).
26. M. Garrad, G. Soter, A. T. Conn, H. Hauser, J. Rossiter, A soft matter computer for soft robots. *Sci. Robot.* **4**, eaaw6060 (2019).
27. W. H. Grover, A. M. Skelley, C. N. Liu, E. T. Lagally, R. A. Mathies, Monolithic membrane valves and diaphragm pumps for practical large-scale integration into glass microfluidic devices. *Sens. Actuators B* **89**, 315–323 (2003).
28. W. H. Grover, R. H. Ivester, E. C. Jensen, R. A. Mathies, Development and multiplexed control of latching pneumatic valves using microfluidic logical structures. *Lab Chip* **6**, 623–631 (2006).
29. M. Rhee, M. A. Burns, Microfluidic pneumatic logic circuits and digital pneumatic microprocessors for integrated microfluidic systems. *Lab Chip* **9**, 3131–3143 (2009).
30. B. Mosadegh, C.-H. Kuo, Y.-C. Tung, Y. Torisawa, T. Mersano-Begey, H. Tavana, S. Takayama, Integrated elastomeric components for autonomous regulation of sequential and oscillatory flow switching in microfluidic devices. *Nat. Phys.* **6**, 433–437 (2010).
31. K. W. Oh, K. Lee, B. Ahn, E. P. Furlani, Design of pressure-driven microfluidic networks using electric circuit analogy. *Lab Chip* **12**, 515–545 (2012).
32. N. S. G. K. Devaraju, M. A. Unger, Pressure driven digital logic in PDMS based microfluidic devices fabricated by multilayer soft lithography. *Lab Chip* **12**, 4809–4815 (2012).
33. M. Wehner, R. L. Truby, D. J. Fitzgerald, B. Mosadegh, G. M. Whitesides, J. A. Lewis, R. J. Wood, An integrated design and fabrication strategy for entirely soft, autonomous robots. *Nature* **536**, 451–455 (2016).
34. S. T. Mahon, A. Buchoux, M. E. Sayed, L. Teng, A. A. Stokes, Soft robots for extreme environments: Removing electronic control, in*2019 2nd IEEE International Conference on Soft Robotics (RoboSoft)* (IEEE, Seoul, Korea, 14 to 18 April 2019), pp. 782–787.
35. P. Rothemund, A. Ainla, L. Belding, D. J. Preston, S. Kurihara, Z. Suo, G. M. Whitesides, A soft, bistable valve for autonomous control of soft actuators. *Sci. Robot.* **3**, eaar7986 (2018).
36. D. Preston, P. Rothemund, H. J. Jiang, M. P. Nemitz, J. Rawson, Z. Suo, G. M. Whitesides, Digital logic for soft devices. *Proc. Natl. Acad. Sci. U.S.A.* **116**, 7750–7759 (2019).
37. D. J. Preston, H. J. Jiang, V. Sanchez, P. Rothemund, J. Rawson, M. P. Nemitz, W.-K. Lee, Z. Suo, C. J. Walsh, G. M. Whitesides, A soft ring oscillator. *Sci. Robot.* **4**, eaaw5496 (2019).
38. P. A. Guertin, Central pattern generator for locomotion: Anatomical, physiological, and pathophysiological considerations. *Front. Neurol.* **3**, 183 (2013).
39. A. Roberts, W.-C. Li, S. R. Soffe, How neurons generate behavior in a hatchling amphibian tadpole: An outline. *Front. Behav. Neurosci.* **4**, 16 (2010).
40. S. Grillner, T. M. Jessell, Measured motion: searching for simplicity in spinal locomotor networks. *Curr. Opin. Neurobiol.* **19**, 572–586 (2009).
41. S. M. Danner, S. D. Wilshin, N. A. Shevtsova, I. A. Rybak, Central control of interlimb coordination and speed-dependent gait expression in quadrupeds. *J. Physiol.* **594**, 6947–6967 (2016).
42. B. Blasing, H. Cruse, Stick insect locomotion in a complex environment: Climbing over large gaps. *J. Exp. Biol.* **207** (Pt 8), 1273–1286 (2004).
43. C. P. Spirito, D. L. Mushrush, Interlimb coordination during slow walking in the cockroach. *J. Exp. Biol.* **78**, 233–243 (1979).
44. T. Buschmann, A. Ewald, A. von Twickel, A. Buschges, Controlling legs for locomotion—Insights from robotics and neurobiology. *Bioinspir. Biomim.* **10**, 041001 (2015).
45. T. Barnes, T. Truong, G. Adams, N. McGruer, large deflection analysis of a biomimetic lobster robot antenna due to contact and flow. *J. Appl. Mech.* **68**, 948–951 (2001).
46. A. J. Ijspeert, Central pattern generators for locomotion control in animals and robots: A review. *Neural Netw.* **21**, 642–653 (2008).
47. T. Umedachi, T. Kano, A. Ishiguro, B. A. Trimmer, Gait control in a soft robot by sensing interactions with the environment using self-deformation. *R. Soc. Open Sci.* **3**, 160766 (2016).
48. K. Luo, P. Rothemund, G. M. Whitesides, Z. Suo, Soft kink valves. *J. Mech. Phys. Solids* **131**, 230–239 (2019).
49. A. Jayes, R. M. Alexander, The gaits of chelonians: Walking techniques for very low speeds. *J. Zool.* **191**, 353–378 (1980).
50. R. Alexander, Optimization and gaits in the locomotion of vertebrates. *Physiol. Rev.* **69**, 1199–1227 (1989).
51. R. M. Alexander, *Optima for Animals* (Princeton Univ. Press, 1996).
52. M. MacKay-Lyons, Central pattern generation of locomotion: A review of the evidence. *Phys. Ther.* **82**, 69–83 (2002).

53. A. Pandey, D. E. Moulton, D. Vella, D. P. Holmes, Dynamics of snapping beams and jumping poppers. *Europhys. Lett.* **105**, 24001 (2014).
54. D. Brown, *Tracker Video Analysis* (2007); http://physlets.org/tracker/.

Acknowledgments: We would like to thank the members of the Bioinspired Robotics and Design Lab for helpful feedback while putting the content together. **Funding:** This work is supported by the Office of Naval Research, grant numbers N00014-17-1-2062 and N00014-18-1-2277. **Author contributions:** D.D., S.J., and M.T.T. designed the experiments and analyzed the results. D.D., S.J., D.S., and C.C. fabricated experimental components and conducted the experiments. D.D. and M.T.T. prepared the manuscript. All authors contributed to, and agree with, the content of the final version of the manuscript. **Competing interests:** D.D., S.J., D.S., C.C., and M.T.T. are inventors on a patent application filed by University of California, San Diego that covers the design of pneumatic circuits for the control of soft-legged robots. **Data and materials availability:** All data needed to evaluate the study are presented in the main text or the Supplementary Materials. Raw data are available from the authors upon request.

Submitted 15 June 2020
Accepted 26 January 2021
Published 17 February 2021
10.1126/scirobotics.aay2627

Citation: D. Drotman, S. Jadhav, D. Sharp, C. Chan, M. T. Tolley, Electronics-free pneumatic circuits for controlling soft-legged robots. *Sci. Robot.* **6**, eaay2627 (2021).

Science Robotics

Electronics-free pneumatic circuits for controlling soft-legged robots

Dylan Drotman, Saurabh Jadhav, David Sharp, Christian Chan, and Michael T. Tolley

Sci. Robot. **6** (51), eaay2627. DOI: 10.1126/scirobotics.aay2627

Science Robotics (ISSN 2470-9476) is published by the American Association for the Advancement of Science. 1200 New York Avenue NW, Washington, DC 20005. The title *Science Robotics* is a registered trademark of AAAS.